HALDER, N. C. & WAGNER, C. N. J. (1967). *Z. Naturforschg.* **22**a, 1489.
HALDER, N. C. & WAGNER, C. N. J. (1968). *Z. Naturforschg.* **23**a, 992.
HULTGREN, R. & ORR, R. L. (1967). *Rev. Int. Hautes Temp. Refract.* **4**, 123.
KAPLOW, R., STRONG, S. L. & AVERBACH, B. L. (1965). *Phys. Rev.* **138**A, 1336.
OCKEN, H. & WAGNER, C. N. J. (1966). *Phys. Rev.* **149**, 122.
RIVLIN, V. G., WAGHORNE, R. M. & WILLIAMS, G. I. (1966). *Phil. Mag.* **13**, 1169.
RUPPERSBERG, H. (1967). *Rev. Int. Hautes Temp. Refract* **4**, 113.
RUPPERSBERG, H. (1969). *Z. Naturforschg.* **24**a, 1034.
RUPPERSBERG, H. (1970). *Z. Naturforschg.* **25**a, 749.
RUPPERSBERG, H. & SEEMANN, H. J. (1965). *Z. Naturforschg.* **20**a, 104.
RUPPERSBERG, H. & WINTERBERG, K. -H. (1971). *Phys. Letters,* **34**A, 11.
SAGEL, K. (1958). *Tabellen zur Röntgenstrukturanalyse,* Berlin: Springer.
THOMAS, L. H. & UMEDA, K. (1957). *J. Chem. Phys.* **26**, 293.
WAGHORNE, R. M., RIVLIN, V. G. & WILLIAMS, G. I. (1967). *Advanc. Phys.* **16**, 215.
WAGNER, C. N. J., OCKEN, H. & JOSHI, M. L. (1965). *Z. Naturforschg.* **20**a, 325.
WASEDA, Y., IIDA, T., SUZUKI, K. & TAKEUCHI, S. (1969). *Phys. Letters,* **29**a, 227.
WASEDA, Y., IIDA, T., SUZUKI, K. & TAKEUCHI, S. (1969). *Phys. Letters,* **30**A, 121.
WASEDA, Y. & SUZUKI, K. (1970), *Phys. Letters,* **31**A, 573.
WASEDA, Y. & SUZUKI, K. (1970). *Phys. stat. sol.* **40**, 183.

Acta Cryst. (1972). A**28**, 236

A Highly Efficient Neutron Diffraction Technique: Use of White Radiation*

BY CAMDEN R. HUBBARD, CARL O. QUICKSALL AND ROBERT A. JACOBSON

Institute for Atomic Research and Department of Chemistry, Iowa State University, Ames, Iowa 50010, *U.S.A.*

(*Received* 5 *March* 1971)

A technique, using a white-radiation neutron beam, has been developed that dramatically increases both counting precision and data-collection rates over conventional monochromatic beam techniques. The theoretical equation of scattering and practical equations for incident flux, absorption correction, and extinction correction are presented. Using a NaCl crystal, the incident flux was found to correspond to a Maxwellian distribution. Using a 5 MW research reactor, 2286 data points were collected in a period of one week from a 2 mm^3, α-oxalic acid dihydrate crystal. Refinement based on all observed intensities produced parameters that were in excellent agreement with literature values. Of the 680 observations with $I > 3\sigma_I$, the weighted R value = 0·102.

Introduction

A major limitation in single-crystal neutron diffraction studies is the relatively low flux of the neutron beams employed. To obtain adequate counting rates, large single crystals are usually required. These crystals are often difficult to obtain and can exhibit appreciable secondary extinction effects. In particular, hydrogen-containing compounds must be deuterated to avoid the strong effective absorption resulting from hydrogen incoherent scattering.

Present inefficient methods contribute greatly to the low flux of the neutron beam. The conventional monochromatic beam technique is poor in this sense. Monochromatic crystals are never totally efficient diffractors and they 'see' only a very small effective source at the reactor core, due to the small mosaic spread of the crystal. The time-of-flight (TOF) technique does not provide an improvement over monochromatic beams, due to the necessarily low efficiency of Fermi choppers. Alternate methods using Fourier choppers (Colwell, Miller & Whittemore, 1968) or correlation choppers (Gompf, Reichardt, Glaser & Beckurts, 1968) are being tested experimentally. These choppers are ≃25% efficient, and a large increase in incident flux can be expected. However, sophisticated electronics are required, and results to date are not impressive.

The Laue diffraction method can be used to greatly increase the incident flux, and, consequently, smaller crystals can be studied at faster data rates. The large increase in flux results from several factors. First, the inefficiency of a crystal monochromator (or chopper) is eliminated. Second, the effective source of the incident beam can be much larger than that 'seen' by a monochromating crystal. Finally, the neutron-path length from the reactor core to the sample crystal can be a minimum since secondary equipment (such as a monochromator or chopper) is eliminated. The diffracted intensity is also enhanced by two other effects. First, each integrated intensity can be measured with a single-peak height measurement (Lowde, 1956) due

* Work was performed in the Ames Laboratory of the U. S. Atomic Energy Commision. Contribution No. 2951.

to a wavelength integration. Second, each Laue intensity consists of a summation of intensities from many structure factors with identical Miller indexes.

The application of the white-radiation neutron spectrum was discussed by Lowde (1951). However, the analysis of the resulting intensities was considered a fundamental weakness of the method. Lowde did not resolve this problem, and a monochromatic beam from a high-flux reactor was considered necessary for neutron diffraction studies of most materials. In the white-radiation method presented here, each Laue intensity is measured at selected scattering angles. By coupling the Θ and Ω diffractometer axes, each Laue intensity may be observed at a wide range of scattering angles, θ, and may be considered a 'Laue streak'. The overlap of intensity from several wavelengths causes minimal difficulty in the data analysis. Structure factors obtainable from observed intensities are used to determine the structural model. This model is subsequently refined by a least-squares analysis based on observed and calculated intensities. Wavelength-dependent corrections for extinction and absorption are included in calculated intensities.

Theory

The mathematical formulation of the intensity equation, extinction correction, absorption correction, and incident flux equation pertinent to the use of a polychromatic neutron beam for crystal-structure determination are given in this section. Corrections for inelastic scattering and multiple Bragg scattering are assumed to be negligible. Techniques for obtaining and refining structural models are also discussed.

Intensity formula

Each Laue spot can be measured at various scattering angles, θ, using a polychromatic beam and the bisecting orientation. The observed intensity consists of a summation of intensities resulting from all structure factors with Miller indexes $\mathbf{h}'=(h'k'l')$ scattering at the same Bragg angle, and

$$I_{\mathbf{h}'}^{\mathrm{obs}}(\theta)=\sum_{n} I_{\mathbf{h}}(\theta)\,, \tag{1}$$

where the crystallographic indexes $\mathbf{h}=(nh',nk',nl')$. Individual intensity terms, $I_{\mathbf{h}}$, are derived below following the procedure of Buras, Giebultowiez, Minor & Rajca (1970) for the TOF spinning-crystal technique.

The integrated intensity for Bragg diffraction using a monochromatic beam-rotating crystal method is given by

$$i_{\mathbf{h}}(\theta)=k\Phi(\lambda)\lambda^3F_{\mathbf{h}}^2T(\lambda)y(\lambda)/\sin 2\theta\,, \tag{2}$$

where k is a scale factor, $F_{\mathbf{h}}$ is the structure factor, $T(\lambda)$ is an absorption correction, $y(\lambda)$ is an extinction correction, θ is the Bragg angle, and $\Phi(\lambda)$ is the flux at wavelength λ. The intensity terms, $I_{\mathbf{h}}(\theta)$, are obtained by integrating $i_{\mathbf{h}}(\theta)$ over the wavelengths accepted by the counter, and

$$I_{\mathbf{h}}(\theta)=k\int_{\lambda_{\min}}^{\lambda_{\max}}\Phi(\lambda)\,\lambda^3F_{\mathbf{h}}^2T(\lambda)y(\lambda)\frac{\mathrm{d}\lambda}{\sin 2\theta}\,, \tag{3}$$

where $\lambda_{\min}$ and $\lambda_{\max}$ are determined by Bragg's equation for the finite counter aperture, 2δ, centered about θ_0. When variable $\mathrm{d}\lambda$ is changed to $\mathrm{d}\theta$ using $\mathrm{d}\lambda=\lambda\cot(\theta)\,\mathrm{d}\theta$ from Bragg's law, and when one realizes that $\Phi(\lambda)$, $y(\lambda)$, $T(\lambda)$ and $\sin^2\theta$ are essentially constants over the small angular range involved,

$$I_{\mathbf{h}}(\theta_0)=k\lambda_n^4\Phi(\lambda_n)F_{\mathbf{h}}^2T(\lambda_n)y(\lambda_n)\delta/\sin^2\theta_0\,, \tag{4}$$

where $\lambda_n=2d_{\mathbf{h}}\sin\theta_0$. By substituting equation (4) in equation (1), defining $\Phi_{\mathrm{eff}}(\lambda)=\lambda^2\Phi(\lambda)$, and replacing $\lambda^2/\sin^2\theta_0$ with $d_{\mathbf{h}}^2$, the final form of the intensity equation is obtained:

$$I_{\mathbf{h}'}(\theta_0)=K\sum_{n}\Phi_{\mathrm{eff}}(\lambda_n)T(\lambda_n)\,(F_{\mathbf{h}}d_{\mathbf{h}})^2\,. \tag{5}$$

Extinction

Since extinction correction varies with wavelength, the correction can be important in the white-radiation method. Assuming that primary extinction can be neglected, the secondary extinction correction can be calculated using the Zachariasen (1967) approximation:

$$y(\lambda)=\left\{1+\frac{2rQ_0\bar{T}}{\lambda\sqrt{1+(r/\lambda g)^2}}\right\}^{-1/2}\,. \tag{6}$$

In this expression, $Q_0=\lambda^3F_c^2/[V_c^2\sin(2\theta)]$, where r and g are the domain radius and Gaussian distribution parameters respectively, and $\bar{T}$ is the absorption-weighted path length.

White-radiation data can be sufficient to determine both r and g simultaneously (Zachariasen, 1968). Often, in practice however either $r\gg\lambda g$ or $\lambda g\gg r$. In either case, the extinction correction is a function of only one parameter:

$$\begin{array}{ll} r\gg g\lambda \\ \text{(type I)} & y(\lambda)=\{1+2gQ_0\bar{T}\}^{-1/2}\,, \\ \\ \lambda g\gg r \\ \text{(type II)} & y(\lambda)=\{1+2rQ_0\bar{T}/\lambda\}^{-1/2}\,. \end{array} \tag{7}$$

Absorption

Attenuation of the incident and diffracted beam within the crystal results from two effects: true absorption and incoherent scattering. The linear absorption coefficient for true absorption, μ^{abs}, varies linearly with wavelength for nearly all elements (exceptions are the highly absorbing elements such as Cd or Gd). This linear relation is

$$\frac{\mu^{\mathrm{abs}}}{\mu_0^{\mathrm{abs}}}=\lambda/\lambda_0\,, \tag{8}$$

where μ^{abs} and μ_0^{abs} correspond to wavelengths λ and λ_0 respectively.

Attenuation due to incoherent scattering is wave-

length-independent for nearly all elements. However, hydrogen is an important exception. In the next section, hydrogen incoherent scattering is shown to increase approximately linearly with wavelength. The cumulative effect of both true absorption and incoherent scattering, expressed in terms of the linear attenuation coefficient, is

$$\mu=\mu^{\text{abs}}+\mu^{\text{incoh}} . \tag{9}$$

The transmission factor $T(\lambda)$ can be calculated for any wavelength by a Taylor series expansion about λ_0:

$$T(\lambda)=T(\lambda_0)+\partial T/\partial\lambda\,|_{\lambda_0}(\lambda-\lambda_0) +\tfrac{1}{2}\partial^2T/\partial\lambda^2\,|_{\lambda_0}(\lambda-\lambda_0)^2\ldots \tag{10}$$

Since $\partial T/\partial\lambda=(\partial T/\partial\mu)(\partial\mu/\partial\lambda)$, equation (10) can be written as

$$T(\lambda)=T(\lambda_0)+\partial T/\partial\mu\,|_{\mu_0}\Delta\mu +\partial^2T/\partial\mu^2\,|_{\mu_0}\Delta\mu^2+\ldots , \tag{11}$$

where

$$\Delta\mu=\partial\mu/\partial\lambda|_{\lambda_0}(\lambda-\lambda_0)=\mu_0'(\lambda/\lambda_0-1) .$$

The attenuation-weighted path length $\bar{T}(\lambda)$, necessary for extinction corrections, can also be calculated from $T(\lambda)$ and derivatives $\partial T/\partial\mu$ and $\partial^2T/\partial\mu^2$:

$$\bar{T}(\lambda)=-\{\partial T/\partial\mu\,|_{\mu_0}+\partial^2T/\partial\mu^2\,|_{\mu_0}\Delta\mu\}/T(\lambda) . \tag{12}$$

Terms $T(\lambda_0)$, $\partial T/\partial\mu\,|_{\mu_0}$ and $\partial^2T/\partial\mu^2\,|_{\mu_0}$ are evaluated by numerical integration.

Hydrogen incoherent scattering

The effective cross section of hydrogen increases with wavelength from the lower (unbound) limit of $\simeq$ 20 b to the upper (bound) limit of $\simeq$ 80 b, over the wavelength range of 0·25 to 4 Å. The particular wavelength dependence was reported by Melkonian (1949) for a variety of gases, water and (*l*) n-butane. In the wavelength range 0·7 to 3·0 Å, the cross section for a chemically bonded hydrogen atom can be represented adequately by

$$\sigma^{\text{H}}\simeq 37+12\left(\frac{\lambda}{\lambda_0}-1\right)\text{b} , \tag{13}$$

where one barn (b) $=10^{-24}$ cm^2 and $\lambda_0=1$ Å.

Subtracting the wavelength-independent Bragg scattering cross section, $\sigma^{\text{coh}}=1{\cdot}8$ b, yields the hydrogen incoherent scattering cross section:

$$\sigma^{\text{H-incoh}}\simeq 35{\cdot}2+12\left(\frac{\lambda}{\lambda_0}-1\right)\text{b} . \tag{14}$$

The wavelength dependence of the linear attenuation coefficient for any compound can be calculated using equation (15), if the true absorption and incoherent scattering cross sections are known:

$$\mu(\text{cm}^{-1})=\frac{1}{V_c}\left\{\sum_i(\sigma^{\text{abs}}+\sigma^{\text{incoh}})\right\} , \tag{15}$$

where V_c is the volume of the unit cell and $\sum$ sums over all atoms in one unit cell. Evaluation of the resulting expression at a reference wavelength, λ_0, gives:

$$\mu(\lambda)=\mu(\lambda_0)+\mu_0'(\lambda/\lambda_0-1) \tag{16}$$

whose form is applicable to the Taylor series expansion for the transmission factor [equation (11)]. The large incoherent scattering cross section for hydrogen will generally dominate in hydrogen-containing compounds.

Effective flux

If the thermal neutrons are fully moderated, the incident flux would be the product of a Maxwellian distribution and an effusion rate (Bacon & Thewlis, 1949). Expressed in terms of wavelength, it is:

$$\Phi_{\text{incid}}\propto\frac{1}{\lambda^5}e^{-P1/\lambda^2} ,$$

where $P1$ is related to the moderator temperature.

Previous work with TOF instruments (Lebech & Mikke, 1967) indicates that the effective detectable flux can be represented by the following general four-parameter equation:

$$\Phi_{\text{eff}}(\lambda)=K(e^{-P1/\lambda^2}/\lambda^{P3})\,e^{-P2\lambda}(1-e^{-P4\lambda}) . \tag{18}$$

The expression $e^{-P2\lambda}$ is added to account for the small absorption of the incident beam by Al windows and air, while the expression $(1-e^{-P4\lambda})$ is a counter efficiency correction. The constant $P4$ can be determined from manufacturer's specifications. The expected beam distribution should be Maxwellian ($P3=3{\cdot}0$).

Obtaining the model

Two methods can be used to obtain structure factors from white-radiation data. The 'observed' structure factors can then be phased by the known fragment and a Fourier series can be calculated. With even approximate amplitudes, the Fourier series often reveals atoms, such as hydrogen, which were not found in a previous X-ray analysis.

The first method to obtain F^2's is a simple approximation technique. The low sin θ data, where only first-order scattering is significant, is solved for $F^2_{1\mathbf{h}'}$. The contribution of $F^2_{1\mathbf{h}'}$ to the observed intensity streak is subtracted, and the process is repeated for $F^2_{2\mathbf{h}'}$, *etc.* Since the error in $F^2_{n\mathbf{h}'}$ increases rapidly with n, this method should be terminated when the error in $F^2_{n\mathbf{h}'}$ is of the same magnitude as $F^2_{n\mathbf{h}'}$ itself. An estimate for the extinction correction is easily included in this technique.

A linear least-squares method can be used when the extinction correction is not large. The system of equations [equation (5)] is rewritten here in matrix form:

$$\mathbf{I}=\mathbf{M}\cdot\{F^2/d^{*2}\} . \tag{19}$$

The vector of m observations along one streak is $\mathbf{I}$, the matrix $\mathbf{M}$ includes flux and transmission factors, and $\{F^2/d^{*2}\}$ is the vector of unknowns.

For $m>n$, these linear equations are easily solved

by a weighted least-squares technique to obtain 'observed' structure factors. Along dense reciprocal lattice rows, the calculated high-order structure factors may exhibit increasing oscillation about zero. Restricting n to $\leq 2 \sin \theta_{max}/(1{\cdot}3d^*)$ has proved adequate to eliminate oscillation. Since only approximate structure factors are necessary to obtain a structural model, this technique should succeed for nearly all problems.

Refining the model

Refinement based on the indirectly 'observed' structure factors is possible. However, refinement of the structural model based on observed intensities is more meaningful and does not require determination of accurate structure factors from the data. To perform this refinement a full-matrix least-squares program *WIRALS* (*WI*te *RA*diation *L*east *S*quares) was written. The quantity minimized is $\sum w_i(I_i^o - I_i^c)^2$. *WIRALS* includes refinement of a scale factor, flux parameters, isotropic extinction parameters, and atomic coordinates and thermal parameters. *WIRALS* uses significant portions of *ORFLS* (Busing, Martin & Levy, 1962) previously modified to include group refinement. *WIRALS* corrects the calculated data for extinction and absorption before comparing calculated and observed intensities. The latter are corrected only for background. All observed data including $I^o < 0$ may be included in the refinement.

Experimental

To experimentally test the white-radiation method, a beam tube of the 5 MW Ames Laboratory Research Reactor was temporarily modified to provide a collimated neutron (and γ) beam at a reactor face. However, due to physical limitations, the diffractometer and biological shielding were located ~ 5 m from the reactor face. An evacuated flight tube was placed between the reactor face and the diffractometer to prevent unnecessary air scattering. A secondary collimator at the diffractometer end of the flight tube defined a $\frac{3}{4}$ in diameter beam with a very small divergence angle.

A conventional four-circle E. & A. diffractometer (similar to an X-ray diffractometer) was carefully aligned and surrounded by concrete and paraffin walls for biological shielding. The diffractometer was fully automated using a DATEX controller and the Ames Laboratory SDS-910 real-time computer system. The diffractometer was equipped with top-bottom left-right beam splitters and a shielded BF_3 detector. The main beam was monitored with a ^{235}U fission counter. Approximately 1 in 10^4 neutrons is detected by this counter. All diffracted-beam counting periods were based on a fixed number of monitor counts.

A spherical NaCl crystal (3·5 mm diameter) was carefully centered and used for final alignment of the diffractometer. To experimentally confirm that integrated intensities can be obtained by peak-height measurements, both peak-height and Ω-scan data were collected. Backgrounds for both intensity measurements were collected at an Ω offset of $\pm 2{\cdot}0°$. As anticipated, the ratio of the peak height to scan intensity data was a constant in the range $10° \geq 2\theta \geq 140°$. This initial study also indicated that much smaller crystals could be used.

The procedure for three-dimensional data collection is as follows. The precise orientation of three noncoplanar Laue reflections is determined using the beam splitters. An orientation matrix is then calculated from the orientation information and calculated reciprocal lattice spacings. During data collection, peak heights of three reflections are periodically remeasured to ensure crystal, flux, and electronic stability. For any particular Laue streak with Miller indexes ($h'k'l'$) scattering angles (θ) are determined by

$$\sin \theta = \frac{n\hat{\lambda}}{2d_{h'}}, \qquad (20)$$

where $n = 1, 2, 3$, *etc.* and $\hat{\lambda}$ = an arbitrary wavelength increment.

The intensity of a Laue streak is measured at each θ determined by equation (20), $5° \leq \theta \leq 70°$, for a fixed number of monitor counts. The background is measured on each side of the Laue streak by offsetting Ω ($\pm \Delta\Omega$) and counting for the same fixed number of monitor counts. Observed intensity and an expected standard deviation are calculated from the peak height (PH) and the two backgrounds (bg1 and bg2) using

$$I^o = \mathrm{PH} - 0{\cdot}5\ (\mathrm{bg1} + \mathrm{bg2})$$

and

$$\sigma_I^2 = \mathrm{PH} + 0{\cdot}25\ (\mathrm{bg1} + \mathrm{bg2}) + (0{\cdot}02I^o)^2 . \qquad (21)$$

The term $(0{\cdot}02I^o)^2$ represents an empirical correction for instrument instability. The fact that the wavelength increment $\hat{\lambda}$ can be arbitrarily selected has one important implication. More independent observations are available using this method, than with a monochromatic beam experiment. This increase in observations provides the possibility of improved refinement of the structural model.

Results

Effective flux

To experimentally measure the effective flux, an NaCl crystal ($1 \times 2 \times 2$ mm) was mounted on an aluminum rod and carefully aligned with X-rays and neutrons. A total of 155 data points was collected for 55 Laue streaks in one octant of the sphere of reflection using a wavelength increment $\hat{\lambda} = 0{\cdot}7$ Å and $\Delta\Omega = \pm 2{\cdot}0°$. Each peak height and background was measured for 10^5 monitor counts ($\simeq 20$ sec).

The linear absorption coefficients for NaCl can be represented by (Bacon, 1962):

$$\mu(\lambda) = 0{\cdot}539 + 0{\cdot}435\left(\frac{\lambda}{1{\cdot}08} - 1\right) \mathrm{cm}^{-1} .$$

Scattering lengths $b_{Na}=3{\cdot}51$ f* and $b_{Cl}=9{\cdot}6$ f [Neutron Diffraction Commission (NDC), 1969] were used in this study. Assuming a Maxwellian distribution ($P3=3{\cdot}0$), a least-squares analysis showed that the data were insensitive to r, the domain radius. The crystal was then assumed to exhibit type I extinction. To check for any deviation from a Maxwellian distribution, parameters k, $P1$, $P2$, g, B_{Na} and B_{Cl} were refined for various values of $P3$. Results and estimated standard deviations derived from a least-squares analysis are listed in Table 1. These results indicate that g, B_{Na} and B_{Cl} are independent of the choice of $P3$. Parameters $P1=2{\cdot}41$ and $P2=0{\cdot}01$ for the Maxwellian distribution compare reasonably with anticipated values† of 2·56 and 0·10 respectively. Fig. 1 shows the effective flux and incident flux for a Maxwellian distribution as calculated by equation (18). Table 2 lists the relative wavelength $n\hat{\lambda}$, $I^{obs}/10$ and $I^{calc}/10$ for $P3=3{\cdot}0$.

Derived thermal parameters $B_{Na}=1{\cdot}90\pm0{\cdot}10$ and $B_{Cl}=1{\cdot}61\pm0{\cdot}06$ agree within 3σ of reported values (Buyers & Smith, 1968). The NaCl study indicates that the effective flux can be adequately described by a simple three-parameter Maxwellian distribution, and that meaningful thermal parameters can be obtained using the white-radiation method.

Refinement of α-$C_2O_4H_2.2H_2O$

The crystal structure of α-oxalic acid dihydrate, hereafter α-POX, was recently studied by neutron diffraction (Sabine, Cox & Craven, 1969) and X-ray diffraction (Delaplane & Ibers, 1969) methods. The study of this structure was expected to be a good test of the white-radiation method, especially since extinction and absorption corrections should be important. The sensitivity of the data to atomic parameters, and a second determination of the effective flux, would also be determined. The lattice constants of Delaplane & Ibers, space group $P2_1/n$ ($Z=2$), $a=6{\cdot}119$, $b=3{\cdot}607$, $c=12{\cdot}057$ Å, $\beta=106°\,19'$, were used in this study.

A crystal of α-POX (2 mm³) was mounted on a quartz rod and was studied with X-rays to ensure the crystal was of good quality. White-radiation neutron data were collected with $\Delta\Omega=\pm2°$ and $\hat{\lambda}=0{\cdot}325$ Å. Since the effective flux is very low for $n\hat{\lambda}=0{\cdot}325$ and 0·650 Å, $n\hat{\lambda}$ was initially set at 0·925 Å. A total of 2290 intensities was collected for 681 Laue streaks in the hkl and $\bar{h}kl$ octants. Four intensities were omitted, as they were obviously misrecorded. Due to the crude temporary experimental arrangement, the background was quite high and only 680 intensities were observed greater than $3\sigma_I$.

The linear absorption coefficient for α-POX was calculated to be $\mu=1{\cdot}66+0{\cdot}53\ (\lambda/\lambda_0-1)$ cm^{-1} at a reference wavelength of 1·08 Å (Bacon, 1962). The range of calculated transmission factors $T(\mu_0)$ was 0·75 to 0·86. Derivatives $\partial T/\partial\mu\,|_{\mu_0}$ and $\partial^2T/\partial\mu^2\,|_{\mu_0}$ were approximately $\frac{1}{10}$ and $\frac{1}{100}$ of $T(\mu_0)$ respectively. E.s.d.'s and observed intensities were calculated as described previously.

The α-POX data for each Laue streak were solved for structure factors, using the approximation technique. Extinction parameter g from prior data refinement was then used in a least-squares analysis for shifts in F^2's. Using these derived F^2's, a Fourier-series calculation phased by the reported carbon and oxygen

* 1 Fermi (f) $=10^{-13}$ cm.

† Calculated assuming the moderator is at 100°C and using an estimated path length for neutrons through air and Al windows.

Table 1. *Refined parameters as a function of* $P3$ *for* NaCl

$P3$	2·5	2·75	3·0	3·25	3·50	Estimated error
K	195·2	192·8	190·7	188·8	187·2	±9
$P1$	2·26	2·33	2·41	2·48	2·55	±0·03
$P2$	0·20	0·10	0·01	−0·08	−0·18	±0·03
g	243·3	235·8	228·8	222·2	215·9	±55
B_{Na}	1·89	1·90	1·90	1·91	1·91	±0·10
B_{Cl}	1·61	1·61	1·61	1·61	1·61	±0·06
C^2*	0·759	0·748	0·740	0·735	0·732	

* $C^2=\sum w_i(I_i^o-I_i^c)^2/(\text{NO}-\text{NV})$, where NO = number of observations, NV = number of variables, and $w_i=1/\sigma_i^2$.

Table 2. $I^{obs}/10$ *and* $I^{calc}/10$ *for* NaCl

$n\hat{\lambda}$	IO	IC	$n\hat{\lambda}$	IO	IC	$n\hat{\lambda}$	IO	IC
••(2, 0, 0)••			1.40	634	631	••(2, 6, 0)••		
0.70	250	263	2.10	389	403	0.70	12	10
1.40	1343	1372	2.80	232	238	1.40	60	54
2.10	942	929	3.50	118	135	••(4, 6, 0)••		
2.80	622	612	••(4, 2, 0)••			0.70	5	6
3.50	405	414	0.70	34	35	1.40	36	30
4.20	283	283	1.40	180	185	••(0, 0, 2)••		
4.90	128	189	2.10	93	102	0.70	235	249
••(0, 2, 0)••			••(6, 2, 0)••			1.40	1326	1243
0.70	257	263	0.70	7	10	2.10	802	837
1.40	1375	1376	1.40	57	54	2.80	619	570
2.10	879	932	••(2, 4, 0)••			3.50	435	404
2.80	622	614	0.70	35	35	4.20	313	291
3.50	423	415	1.40	198	185	4.90	216	208
4.20	287	283	2.10	91	102	••(2, 0, 2)••		
4.90	204	190	••(6, 4, 0)••			0.70	99	114
••(2, 2, 0)••			0.70	9	6	1.40	572	584
0.70	120	119	1.40	30	30	2.10	356	374

$n\hat{\lambda}$	IO	IC	$n\hat{\lambda}$	IO	IC	$n\hat{\lambda}$	IO	IC
2.80	224	229	2.10	563	572	0.70	3	2
3.50	130	141	2.80	516	502	1.40	-15	8
••(4, 0, 2)••			3.50	386	382	••(0, 4, 2)••		
0.70	36	34	4.20	284	281	0.70	40	35
1.40	176	175	4.90	205	204	1.40	173	182
2.10	98	100	5.60	143	151	2.10	98	99
••(6, 0, 2)••			••(4, 2, 2)••			••(2, 4, 2)••		
0.70	10	10	0.70	27	26	0.70	26	26
1.40	45	52	1.40	135	136	1.40	136	137
••(0, 2, 2)••			••(3, 1, 1)••			••(4, 4, 2)••		
0.70	113	118	0.70	14	18	0.70	18	13
1.40	634	609	1.40	103	105	1.40	60	66
2.10	400	380	2.10	92	94	••(0, 6, 2)••		
2.80	232	219	2.80	81	70	0.70	14	10
3.50	142	136	••(5, 1, 1)••			1.40	52	53
••(1, 1, 1)••			0.70	4	5	••(1, 3, 1)••		
0.70	54	79	1.40	24	28	0.70	13	18
1.40	467	487	••(7, 1, 1)••			1.40	107	106

$n\hat{\lambda}$	IO	IC	$n\hat{\lambda}$	IO	IC	$n\hat{\lambda}$	IO	IC
2.10	99	95	••(1, 7, 1)••			0.70	8	13
2.80	73	71	0.70	0	2	1.40	70	66
••(3, 3, 1)••			1.40	11	8	••(2, 4, 4)••		
0.70	8	9	••(2, 0, 4)••			0.70	9	13
1.40	53	49	0.70	39	34	1.40	64	65
2.10	39	36	1.40	180	179	••(0, 6, 4)••		
••(5, 3, 1)••			2.10	103	106	0.70	5	6
0.70	2	3	••(6, 0, 4)••			1.40	32	30
1.40	23	18	0.70	8	6	••(2, 0, 6)••		
••(1, 5, 1)••			1.40	32	30	0.70	10	10
0.70	5	5	••(0, 2, 4)••			1.40	54	54
1.40	32	28	0.70	38	34	••(4, 0, 6)••		
••(3, 5, 1)••			1.40	175	178	0.70	9	6
0.70	6	3	2.10	97	103	1.40	29	31
1.40	19	18	••(2, 2, 4)••			••(0, 2, 6)••		
••(5, 5, 1)••			0.70	24	26	0.70	7	10
0.70	3	2	1.40	132	134	1.40	58	54
1.40	3	8	••(4, 2, 4)••			••(1, 1, 3)••		

$n\hat{\lambda}$	IO	IC	$n\hat{\lambda}$	IO	IC	$n\hat{\lambda}$	IO	IC
0.70	17	18	••(5, 3, 3)••			••(1, 3, 5)••		
1.40	102	102	0.70	6	2	0.70	0	3
2.10	91	93	1.40	14	12	1.40	17	18
2.80	79	72	••(1, 5, 3)••			••(3, 3, 5)••		
••(3, 1, 3)••			0.70	7	3	0.70	0	2
0.70	13	9	1.40	17	18	1.40	11	12
1.40	43	48	••(3, 5, 3)••			••(1, 5, 5)••		
2.10	39	36	0.70	3	2	0.70	2	2
••(5, 1, 3)••			1.40	12	12	1.40	8	8
0.70	1	3	••(1, 1, 5)••			••(1, 1, 7)••		
1.40	20	17	0.70	4	5	0.70	1	2
••(0, 4, 6)••			1.40	25	28	1.40	7	8
0.70	6	6	••(3, 1, 5)••					
1.40	31	30	0.70	2	3			
••(1, 3, 3)••			1.40	13	18			
0.70	12	9	••(5, 1, 5)••					
1.40	51	48	0.70	1	2			
2.10	34	36	1.40	6	[illegible]			

positions (Sabine *et al.*, 1969) clearly revealed all hydrogen atom positions. Subsequent analysis of the high-resolution data was best represented by type I extinction. In this analysis, both kF^2 and g/k were well-determined.

The starting model for least-squares refinement consisted of the atomic parameters reported by Sabine, *et al.* (1969), flux parameters from the NaCl refinement, and $g=5000$. Scattering lengths used were $b_H=-3{\cdot}72$, $b_C=6{\cdot}65$ and $b_O=5{\cdot}77$ f (NDC, 1969). The 2286 data were refined using anisotropic thermal parameters and a type I extinction correction until all shifts were less than 0·01 times the corresponding estimated error. Final measures of fit* were $RI_w(I>3\sigma)=0{\cdot}102$ and $RI_w=0{\cdot}154$. Final flux parameters were $P1=2{\cdot}55$ and $P2=0{\cdot}06$ for $P3=3{\cdot}0$, which agree quite well with the predicted values of 2·56, 0·1 and 3·0 respectively (moderator at 100°C). Small differences between the flux parameters for α-POX and NaCl (2·41, 0·01, 3·0) are thought to be due to refueling the reactor between investigations.

* The conventional weighted R value is generally based on structure factors, not intensities, and is a poor measure of fit when a large fraction of the data is 'unobserved.' To avoid confusion, the weighted R based on intensities will be $RI_w=\{\sum_i w_i (I_i^o-I_i^c)^2/\sum_i w_i (I_i^o)^2\}^{1/2}$. For comparison with other studies based on observed data, RI_w is also reported for only that data with $I>3\sigma$.

Table 3. *Fractional positional parameters of all atoms and their e.s.d.'s*

(All parameters and e.s.d.'s are expressed × 10⁴)

		Present work	Neutron†	X-ray‡
O(1)	x	854 (6)	847 (4)	848 (1)
	y	−574 (13)	−599 (6)	−600 (3)
	z	1493 (3)	1488 (2)	1481 (1)
O(2)	x	−2193 (7)	−2197 (3)	−2201 (1)
	y	2328 (12)	2310 (6)	2305 (2)
	z	360 (3)	360 (2)	361 (1)
O(3)	x	−4525 (8)	−4509 (4)	−4512 (2)
	y	6107 (15)	6136 (6)	6151 (2)
	z	1797 (5)	1799 (2)	1800 (1)
C(1)	x	−466 (5)	−452 (2)	−454 (2)
	y	559 (10)	547 (4)	548 (3)
	z	509 (2)	510 (1)	511 (1)
H(1)	x	262 (11)	293 (7)	357 (20)
	y	83 (21)	93 (12)	−47 (43)
	z	2191 (6)	2189 (3)	2087 (12)
H(2)	x	−5742 (12)	−5740 (7)	−5588 (23)
	y	6932 (23)	6864 (13)	6587 (45)
	z	1166 (6)	1142 (3)	1205 (16)
H(3)	x	−3637 (12)	−3599 (9)	−3869 (31)
	y	4450 (25)	4447 (14)	4508 (52)
	z	1510 (7)	1508 (4)	1584 (18)

† Sabine, Cox & Craven (1969).
‡ Delaplane & Ibers (1969).

Final atomic coordinates, along with those reported previously from neutron (Sabine *et al.*, 1969) and X-ray (Delaplane & Ibers, 1969) investigations, are listed in Table 3. Similarly, final thermal parameters are compared in Table 4. In both cases, e.s.d.'s were obtained from the least-squares analysis. Atomic parameters determined by the white-radiation method essentially all agree within 4σ of the parameters reported by Sabine *et al.*, 1969. Since extinction corrections were not applied in the previous neutron study, the agreement of parameters is considered excellent. Observed and calculated intensities are listed in Table 5. The

Table 4. *Thermal parameters* of all atoms and their e.s.d.'s*

(All parameters and e.s.d.'s are expressed × 10⁴)

		Present work	Neutron†	X-ray‡
O(1)	β_{11}	194 (12)	228 (6)	246 (3)
	β_{22}	698 (42)	827 (18)	1019 (10)
	β_{33}	34 (3)	29 (1)	37 (1)
	β_{12}	137 (21)	143 (7)	141 (4)
	β_{13}	30 (5)	19 (2)	26 (1)
	β_{23}	29 (10)	7 (3)	9 (2)
O(2)	β_{11}	179 (12)	214 (6)	226 (3)
	β_{22}	772 (43)	838 (17)	974 (10)
	β_{33}	39 (3)	32 (1)	49 (1)
	β_{12}	150 (20)	184 (7)	158 (4)
	β_{13}	35 (5)	26 (2)	39 (1)
	β_{23}	30 (10)	7 (3)	13 (2)
O(3)	β_{11}	204 (15)	219 (6)	230 (4)
	β_{22}	818 (51)	829 (17)	1007 (15)
	β_{33}	40 (4)	33 (1)	46 (1)
	β_{12}	64 (23)	69 (8)	104 (5)
	β_{13}	41 (6)	31 (2)	35 (1)
	β_{23}	7 (10)	22 (3)	22 (2)
C(1)	β_{11}	124 (7)	169 (4)	180 (3)
	β_{22}	468 (32)	462 (11)	575 (11)
	β_{33}	32 (2)	27 (1)	42 (1)
	β_{12}	24 (16)	49 (4)	−10 (5)
	β_{13}	21 (3)	21 (1)	22 (1)
	β_{23}	6 (8)	1 (2)	−1 (2)
H(1)	β_{11}	265 (20)	285 (10)	305 (54)
	β_{22}	632 (66)	945 (29)	1463 (183)
	β_{33}	48 (6)	45 (2)	70 (14)
	β_{12}	2 (32)	58 (14)	−12 (78)
	β_{13}	32 (8)	32 (4)	−76 (22)
	β_{23}	0 (18)	4 (6)	76 (43)
H(2)	β_{11}	251 (22)	314 (12)	281 (59)
	β_{22}	1028 (86)	1083 (35)	1868 (238)
	β_{33}	44 (6)	50 (3)	96 (17)
	β_{12}	150 (38)	105 (17)	200 (86)
	β_{13}	11 (10)	24 (4)	51 (27)
	β_{23}	99 (19)	47 (7)	15 (49)
H(3)	β_{11}	287 (25)	343 (13)	608 (91)
	β_{22}	1159 (91)	1097 (40)	1134 (252)
	β_{33}	96 (8)	79 (3)	172 (25)
	β_{12}	240 (43)	126 (19)	227 (110)
	β_{13}	95 (12)	66 (5)	−75 (37)
	β_{23}	−101 (24)	15 (9)	210 (63)

* Form for the anisotropic temperature factor correction is: $\exp[-(\beta_{11}h^2+\beta_{22}k^2+\beta_{33}l^2+2\beta_{12}hk+2\beta_{13}kl+2\beta_{23}hl)]$.
† Sabine, Cox & Craven (1969)
‡ Delaphine & Ibers (1969).

extinction constant g was refined to $12{\cdot}7\times10^3\pm0{\cdot}8\times10^3$. The successful refinement of α-POX indicates that omission of corrections for inelastic scattering and multiple Bragg scattering was justified.

Discussion

Methods for improving the experimental design, and further applications of the white-radiation method, are discussed in this section.

Experimental improvements

Air scattering of the incident beam is the primary source of background. The temporary experimental design used in these studies can be readily modified to use a smaller beam cross section and smaller counter aperture. This modification reduces the background considerably. The smaller counter aperture also improves diffractometer resolution. Background measurements with an Ω offset of $\pm2°$ are satisfactory, if the reciprocal lattice is not too dense. However, a background measurement in the proximity of a neighboring Laue streak must be avoided. An Ω offset of $\pm1°$ is easily obtainable and should suffice for most problems.

In our new experimental arrangement, the incident beam has a variable cross section of up to 5 mm and an included divergence angle of up to 1°. The sample crystal is centered only 1 m from the reactor face. Improved collimation design and shielding materials further reduce the background. The incident flux is predicted to be an order of magnitude more intense and the peak-to-background ratio is increased by a factor of five.

The presence of long wavelength (>2 Å) neutrons in the incident beam contributes to several difficulties in data collection and analysis. Since air scattering increases with wavelength, the background can be decreased if the long wavelength neutron flux is reduced. Both extinction and absorption corrections also increase with increasing wavelength. To partially eliminate these complications a wavelength selective filter is necessary.

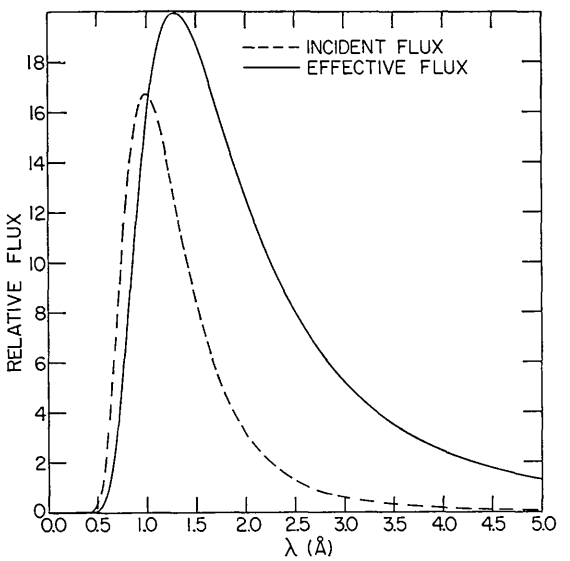

Fig. 1. Incident and effective flux distribution.

A convenient filter is an Eu–Al alloy (6·5 wt%Eu). The theoretical transmission factors, based on the Eu cross section through a 1 mm foil, are 0·90 at 1 Å and 0·49 at 3 Å. To test such a foil, 420 data points were collected along one Laue streak of NaCl with the incident beam filtered (f) and unfiltered (uf). Least-squares analysis determined both $\Phi(\lambda)_f$ and $\Phi(\lambda)_{uf}$. The RI_w were 0·050 and 0·057 respectively. The calculated ratio of $\Phi(\lambda)_f$ to $\Phi(\lambda)_{uf}$ is 0·95 at 1 Å and 0·52 at 3 Å. These results indicate that use of this filter should improve both data collection and analysis.

Further applications

The application of the white-radiation method to other scattering problems is also possible. For example, the study of magnetic ordering is feasible with this technique, which we demonstrated with the use of a $2\times2\times25$ mm Cr crystal, mounted on our single-crystal diffractometer. The magnetic lattice of antiferromagnetic Cr has been reported by Corliss, Hastings & Weiss (1959) to be $(28)^3$ times larger than the *bcc* nuclear lattice. Magnetic satellites about the 100 reciprocal lattice point were calculated to occur at $\Delta\Omega=\pm2{\cdot}1°$. Partial overlap of nuclear and magnetic scattering was anticipated due to the 1·7° resolution of our diffractometer.

Ω scans across the 100 Laue spot are reproduced in Fig. 2(*a*) and (*b*) for scattering angles of 12·5 and 20·0° respectively. Each observation was based on 10^5 monitor counts ($\simeq$20 sec). At $\theta=20°$ the Bragg diffraction from the 200 nuclear planes begins to obscure the magnetic satellites. Our measurements indicate that magnetic scattering can, indeed, be studied efficiently using the white-radiation technique.

If reciprocal space can be accurately mapped by unfolding the observed intensity streak, then inelastic scattering, liquid and powder diffraction studies could be performed using the white-radiation method. Least-squares techniques using auxiliary conditions are currently being studied as a means to achieve this unfolding. Thermal-energy total cross sections can also be measured, using a polychromatic beam transmitted through the sample and analyzed *via* a conventional crystal. Compared with TOF techniques, much higher intensities should be obtained.

Conclusion

The successful structure refinement of α-POX using white-radiation data demonstrates that this new method is a dramatic development in single-crystal neutron diffraction techniques. No other method developed or proposed can realize the efficient use of the

Table 5. I^{obs} *and* I^{calc} *for* α-POX

Table 5 (*cont.*)

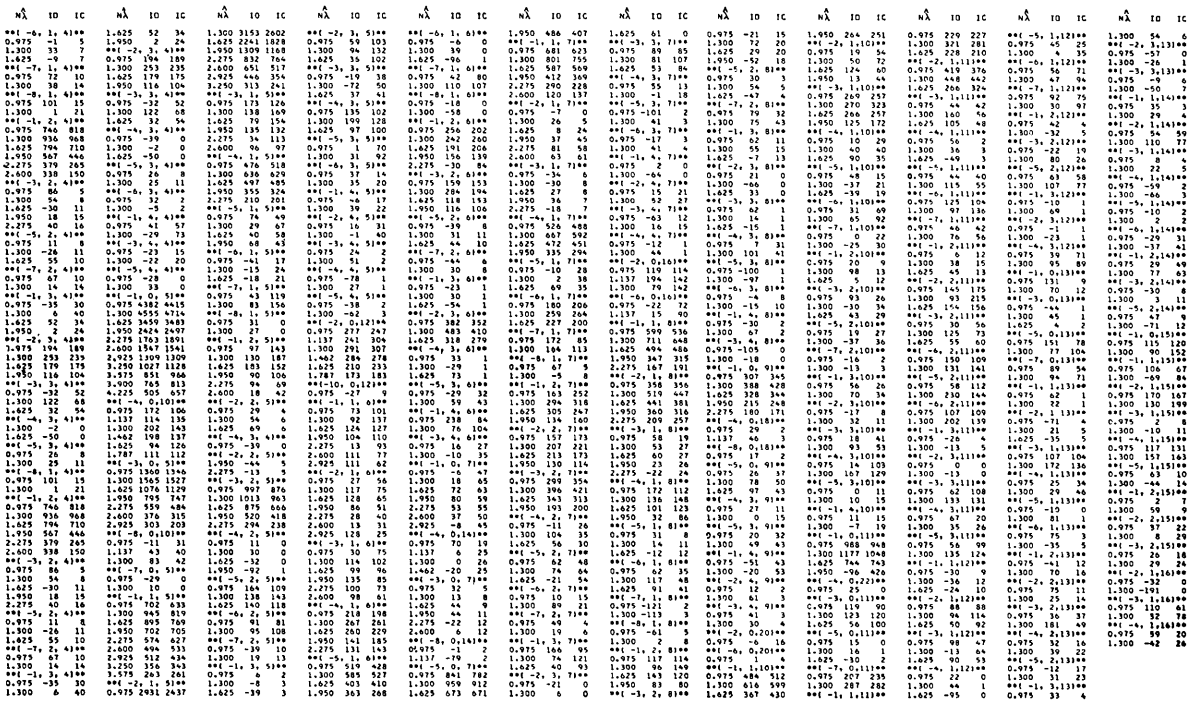

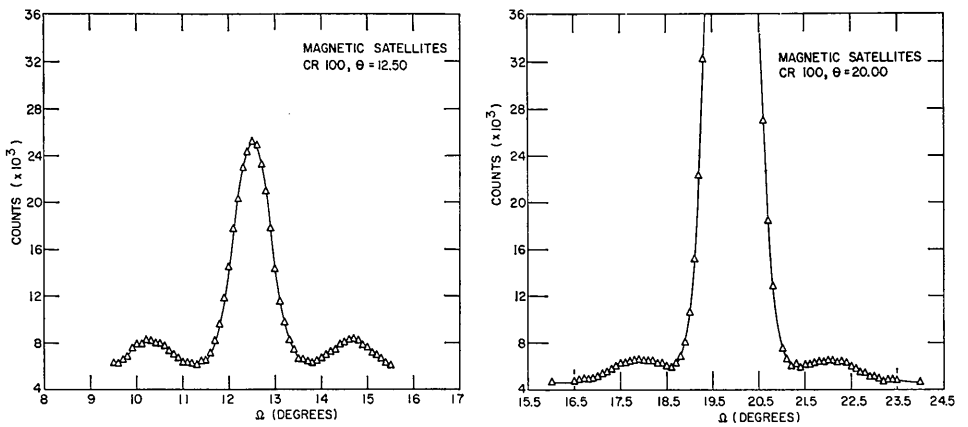

(*a*) (*b*)

Fig. 2. Antiferromagnetic chromium 100 magnetic satellites; (*a*) $\theta = 12{\cdot}5°$, (*b*) $\theta = 20{\cdot}0°$.

thermal neutron spectrum obtained by this method. The large increase in efficiency over conventional methods enables the experimenter to study much smaller crystals at faster data rates without sacrificing experimental precision. This reduction in necessary crystal size permits a much wider variety of compounds to be studied by neutron diffraction.

References

BACON, G. E. (1962). *Neutron Diffraction*, p. 31, 61. Oxford Univ. Press.

BACON, G. E. & THEWLIS, J. (1949). *Proc. Roy. Soc.* **A196**, 50.

BURAS, B., GIEBULTOWIEZ, T., MINOR, W. & RAJCA, A. (1970). *Nucl. Instrum. Meth.* **77**, 13.

BUSING, W. R., MARTIN, K. O. & LEVY, H. A. (1962). Report ORNL-TM-305, Oak Ridge National Laboratory, Oak Ridge, Tennessee.

BUYERS, W. J. L. & SMITH, T. (1968). *J. Phys. Chem. Solids*, **29**, 1051.

COLWELL, J. F., MILLER, P. H. & WHITTEMORE, W. L. (1968). *Neutron Inelastic Scattering*, Vol. II, p. 429–437. International Atomic Energy Agency, Vienna, Austria.

CORLISS, L. M., HASTINGS, J. M. & WEISS, R. J. (1959). *Phys. Rev. Letters*, **3**, 211.

DELAPLANE, R. G. & IBERS, J. A. (1969). *Acta Cryst.* **B25**, 2423.

GOMPF, F., REICHARDT, W., GLASER, W. & BECKURTS, K. H. (1968). *Neutron Inelastic Scattering*, Vol. II, p. 417–428. International Atomic Energy Agency, Vienna, Austria.
LEBECH, B. & MIKKE, K. (1967). Riso Report No. 164. Danish Atomic Energy Commission, Riso, Roskilde, Denmark.
LOWDE, R. D. (1951). *Nature, Lond.* **167**, 243.
LOWDE, R. D. (1956). *Acta Cryst.* **9**, 151.
MELKONIAN, E. (1949). *Phys. Rev.* **76**, 1750.
NENTRON DIFFRACTION COMMISSION (1969). *Acta Cryst.* A**25**, 391.
SABINE, T. M., COX, G. W. & CRAVEN, B. M. (1969). *Acta Cryst.* B**25**, 2437.
ZACHARIASEN, W. H. (1967). *Acta Cryst.* **23**, 558.
ZACHARIASEN, W. H. (1968). *Acta Cryst.* A**24**, 212, 324, 425.

Acta Cryst. (1972). A**28**, 245

Optical Anisotropies of Some Organic Molecules

BY M. A. LASHEEN AND A. M. ABDEEN

Physics Department, Faculty of Science, Alexandria University, Alexandria, U.A.R.

(*Received* 25 *June* 1971 *and in revised form* 7 *November* 1971)

The principal refractive indices of some organic aromatic crystals of known structure have been measured and the principal molecular refractivities deduced from these and the molecular orientation. The substances investigated include aromatic compounds having three rings, two rings or one ring with different substituents. The results give a clear indication that strong magnetic anisotropy is always associated with strong optical anisotropy.

Introduction

Anisotropic properties may often be used to give direct information about the general shape of the molecules in crystals and the way in which the molecules or ions are packed.

The gram molecular refractivity R_M of any crystal can be determined using the Lorentz–Lorenz equation

$$R_M = \frac{(n^2-1)\,M}{(n^2+2)\,D}$$

where n is the refractive index of the crystal, M is the molecular weight and D is the density in g.cm^{-3}. n was measured using the Becke method for the sodium D line at room temperature (about 25 °C).

The molecular refractivity of benzene, and hence the molecular anisotropy Δr were given by Hartshorne & Stuart (1960) to be,

$$\Delta r = \tfrac{1}{2}(r_L + r_M) - r_N = 15{\cdot}7$$

where r_L and r_M are the molecular refractivities in the plane of the molecule and r_N perpendicular to it.

In the case of orthorhombic crystals the crystal refractivities are R_a, R_b and R_c in the direction of the a, b and c axes respectively. For monoclinic crystals the crystal refractivity parallel to [010] is taken as R_3, while R_1 and R_2 denote those in the (010) plane. The sum of R_a, R_b and R_c or R_1, R_2 and R_3 for a crystal is equal to the sum of r_L, r_M and r_N for the molecule.

The transformations from crystalline to molecular refractivities were carried out by the use of the molecular direction cosines obtained from the X-ray crystal structure and the mathematical relations given by Lonsdale & Krishnan (1936).

Orthorhombic crystals

(1) *Triphenylbenzene* $(C_6H_5)_3C_6H_3$

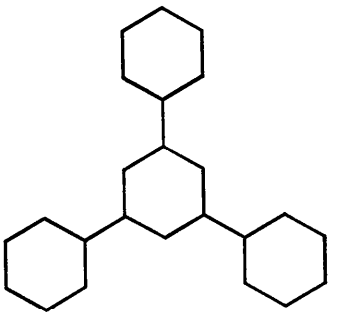

The crystal structure was determined by Farag (1954) who gave:

$a = 7{\cdot}47$, $b = 19{\cdot}66$, $c = 11{\cdot}19$ Å; $Z = 4$; $Pna2_1$.

The crystals used were crystallized from ether.

The principal refractive indices of triphenylbenzene, for the sodium D line are:

Winchell (1943) $n_x = 1{\cdot}5241$, $n_y = 1{\cdot}8670$, $n_z = 1{\cdot}8725$.
Present work $n_a = 1{\cdot}509$, $n_b = 1{\cdot}843$, $n_c = 1{\cdot}849$.

The gram molecular refractivities of triphenylbenzene crystal, where $M = 306{\cdot}14$ and $D = 1{\cdot}237$, are

$$R_a = 73{\cdot}89, \quad R_b = 109{\cdot}89, \quad R_c = 110{\cdot}46.$$